ResearchGate

See discussions, stats, and author profiles for this publication at: https://www.researchgate.net/publication/267274706

Supported copper–copper oxide nanoparticles as active, stable and low-cost catalyst in the methanolysis of ammonia–borane for chemical hydrogen storage

ARTICLE *in* APPLIED CATALYSIS B ENVIRONMENTAL · APRIL 2015

Impact Factor: 7.44 · DOI: 10.1016/j.apcatb.2014.10.011

CITATIONS
11

READS
213

5 AUTHORS, INCLUDING:

Mehmet Yurderi
Yuzuncu Yil University
22 PUBLICATIONS **51** CITATIONS
SEE PROFILE

Ahmet Bulut
Yuzuncu Yil University
21 PUBLICATIONS **51** CITATIONS
SEE PROFILE

Mehmet Zahmakıran
Yuzuncu Yil University
75 PUBLICATIONS **1,590** CITATIONS
SEE PROFILE

Available from: Mehmet Zahmakıran
Retrieved on: 26 January 2016

Applied Catalysis B: Environmental 165 (2015) 169–175

Contents lists available at ScienceDirect

Applied Catalysis B: Environmental

journal homepage: www.elsevier.com/locate/apcatb

Supported copper–copper oxide nanoparticles as active, stable and low-cost catalyst in the methanolysis of ammonia–borane for chemical hydrogen storage

Mehmet Yurderi[a], Ahmet Bulut[a], İlknur Efecan Ertas[a], Mehmet Zahmakiran[a,*], Murat Kaya[b]

[a] Department of Chemistry, Science Faculty, Yüzüncü Yıl University, 65080 Van, Turkey
[b] Department of Chemical Engineering and Applied Chemistry, Atilim University, 06836 Ankara, Turkey

ARTICLE INFO

Article history:
Received 11 July 2014
Received in revised form
25 September 2014
Accepted 3 October 2014
Available online 12 October 2014

Keywords:
Ammonia–borane
Hydrogen storage
Methanolysis
Cuprous oxide
Copper Oxide

ABSTRACT

The physical mixture of copper (Cu) copper(I) oxide (Cu_2O) and copper(II) oxide (CuO) nanoparticles supported on activated carbon (Cu–Cu_2O–CuO/C) were reproducibly prepared by a simple deposition-reduction technique without using any stabilizer in water at room temperature. The characterization of the resulting material by ICP-OES, P-XRD, XPS, DR-UV/vis, BFTEM and HRTEM techniques reveals that the formation of well-dispersed highly crystalline 3.8 ± 1.7 nm nanoparticles on the surface of activated carbon. These carbon supported Cu–Cu_2O–CuO nanoparticles were employed as heterogeneous catalyst in the methanolysis of ammonia–borane (NH_3BH_3), which has been considered as one of the attractive materials for the efficient storage of hydrogen, under mild conditions. We found that only 3.0 mol % Cu–Cu_2O–CuO/C catalyst is enough to catalyze the methanolysis of ammonia–borane with high activity (TOF = 24 min^{-1}) and conversion (>99%) at room temperature. More importantly, the exceptional stability of supported Cu–Cu_2O–CuO nanoparticles against to sintering and leaching make Cu–Cu_2O–CuO/C recyclable catalyst for the methanolysis of ammonia–borane. Cu–Cu_2O–CuO/C catalyst retains >76% of its initial activity with 94% of conversion even at 8th recycle in the methanolysis of ammonia–borane at complete conversion. The study reported here also includes the collection of kinetic data for Cu–Cu_2O–CuO/C catalyzed methanolysis of ammonia–borane depending on catalyst [Cu], substrate [NH_3BH_3] concentrations and temperature to determine the rate expression and the activation parameters (E_a, $\Delta H^{\#}$, and $\Delta S^{\#}$) of the catalytic reaction.

© 2014 Published by Elsevier B.V.

1. Introduction

Hydrogen has been considered as a promising and clean energy carrier [1,2] for our future society as it has a high energy density (142 MJ/kg) almost three times higher than that of natural gas (55 MJ/kg) and only water plus small amounts of heat are the byproducts when it is utilized in proton exchange membrane fuel cells (PEMFC) [3,4]. However, controlled storage and release of hydrogen are still technological barriers in the transition from fossil fuels to hydrogen-based fuel cells energy technologies [1–4]. At this concern, a numerous studies have been performed for the development of materials with high volumetric and gravimetric hydrogen storage capacity, as the low density of hydrogen makes it difficult to store in compressed or liquefied form [5]. In line with this, various porous materials [6–9], boron based chemical hydrides [10–12] and boron–nitrogen compounds [13,14,15–17] have been tested for the chemical hydrogen storage. Among these materials, ammonia–borane (or borane–ammonia complex; AB; NH_3BH_3) has been found to be much better suited for this purpose due to the following advantages: (i) AB has high gravimetric hydrogen storage capacity (19.6 wt%), (ii) it has low molecular weight (30.7 g mol^{-1}), (iii) it is non-flammable and non-explosive under standard conditions [18]. These significant properties make AB unique compared to metal hydrides/B–N compounds or porous materials, where the hydrogen release and uptake can be controlled by temperature and pressure.

Although hydrogen can be released from AB through its' thermal decomposition [19] or dehydrocoupling [20] there is much interest in the transition metal catalyzed hydrolytic dehydrogenation (**1**) due to favorable kinetics and mild reaction conditions [21].

* Corresponding author. Tel.: +90 432 225 22 38; fax: +90 432 225 18 06.
E-mail address: zmehmet@yyu.edu.tr (M. Zahmakiran).

http://dx.doi.org/10.1016/j.apcatb.2014.10.011
0926-3373/© 2014 Published by Elsevier B.V.

However, the hydrolysis of AB in concentrated solutions can cause liberation of ammonia gas that can act as poison to Pt-based fuel cell catalysts [22] and the hydrolysis product of AB is not recyclable due to the strong B–O bonds [14]. These two important issues hinder the practical use of AB-hydrolysis for hydrogen generation system to PEMFCs. In their recent study [23], Ramachandran and co-workers have shown that both problems can be circumvented by using methanol instead of water, as the catalytic methanolysis of ammonia–borane (**2**) yields hydrogen gas without ammonia evolution, and the methanolysis product, ammonium tetramethoxyborate, is recyclable.

$$NH_3BH_3 + 2H_2O \rightarrow NH_4BO_2 + 3H_2 \quad (1)$$

$$NH_3BH_3 + 4CH_3OH \rightarrow NH_4B(OCH_3)_4 + 3H_2 \quad (2)$$

Up to date many heterogeneous catalysts including $RuCl_3$, $RhCl_3$, $PdCl_2$, $CoCl_2$ [23], Cu@Cu_2O [24], Co–Co_2B, Ni–Ni_2B, Co–Ni–B [25], PVP-stabilized Pd(0) [26] Ru(0) NPs [27], CoPd/C [28], intrazeolite Rh(0) NPs [29] and montmorillonite confined Ru(0) NPs [30] have been tested in the methanolysis of ammonia–borane. Unfortunately, most of them used in these schemes suffer from difficult isolation [23–27], low activity [24–28], low stability [23–25,29] or high costs of metals [23,29]. Therefore, the development of highly active, stable and low-cost catalyst that operates under mild conditions remains a challenge in the field.

Herein, we report a facile synthesis of the physical mixture of copper (Cu) copper(I) oxide (Cu_2O) and copper(II) oxide (CuO) nanoparticles (NPs) supported on activated carbon, hereafter referred to as Cu–Cu_2O–CuO/C, and their excellent catalysis in the AB methanolysis. Cu–Cu_2O–CuO/C catalyst was simply and reproducibly prepared through the conventional impregnation followed by simultaneous reduction method [31], and characterized by inductively coupled plasma-optical emission spectroscopy (ICP-OES), powder X-ray diffraction (PXRD), X-ray photoelectron spectroscopy (XPS), diffuse reflectance UV-vis (DR-UV/vis), bright field transmission electron microscopy (BFTEM) and high resolution transmission electron microscopy (HRTEM). The sum of their results revealed that the formation of well-dispersed 3.8 ± 1.7 nm Cu–Cu_2O–CuO NPs on the surface of activated carbon. The resulting Cu–Cu_2O–CuO/C is acting as highly active (TOF = 24 min^{-1}) heterogeneous catalyst in the methanolysis of ammonia–borane at 25 °C. Moreover, the exceptional durability of supported Cu–Cu_2O–CuO NPs against to sintering and leaching make Cu–Cu_2O–CuO/C recyclable catalyst for the methanolysis of ammonia–borane. To the best of our knowledge, this is the first supported catalyst that contains only first-row transition metal and shows remarkable activity and stability in the methanolysis of AB.

2. Experimental

2.1. Materials

Copper(II) chloride dihydrate ($CuCl_2.2H_2O$), copper powder (Cu ~99.99%), copper(I) oxide (Cu_2O ~99.99%), copper(II) oxide (CuO ~99.99%), ammonia–borane (NH_3BH_3 ~90%), sodium borohydride ($NaBH_4$), boron trifluoride diethyl etherate ($BF_3{\cdot}(C_2H_5)_2O$), methanol (CH_3OH) and activated carbon were purchased from Sigma–Aldrich®. Methanol was distilled over Mg and stored in a Schlenk tube under argon atmosphere. Deionized water was distilled by water purification system (Milli-Q Water Purification System). All glassware and Teflon-coated magnetic stir bars were washed with acetone and copiously rinsed with distilled water before drying in an oven at 150 °C.

2.2. Characterization

Cu contents of the samples were determined by ICP-OES (Leeman, Direct Reading Echelle) after each sample was completely dissolved in a mixture of HNO_3/HCl (1/3 ratio). Powder X-ray diffraction (XRD) patterns were recorded with a MAC Science MXP 3TZ diffractometer using Cu-Kα radiation (wavelength 1.54 Å, 40 kV, 55 mA). BFTEM and HRTEM samples were prepared by dropping one drop of dilute suspension on copper coated carbon TEM grid and the solvent was then dried. The conventional TEM was carried out on a JEOL JEM-200CX transmission electron microscopes operating at 120 kV. HRTEM analyses were run on a JEOL JEM-2010F transmission electron microscope operating at 200 kV. The XPS analyses were performed on a Physical Electronics 5800 spectrometer equipped with a hemispherical analyzer and using monochromatic Al-Kα radiation (1486.6 eV, the X-ray tube working at 15 kV and 350 W, and pass energy of 23.5 eV). DR-UV/vis analyses were performed on Shimadzu UV-3600 modulated with integrating sphere attachment. ^{11}B NMR spectra were recorded on a Bruker Avance DPX 400 with an operating frequency of 128.15 MHz. CD_3OD and $BF_3{\cdot}(C_2H_5)_2O$ were used as a lock and an external reference, respectively. At the end of the methanolysis reaction, the resulting solutions were filtered and the filtrates were collected for taking the ^{11}B NMR spectra.

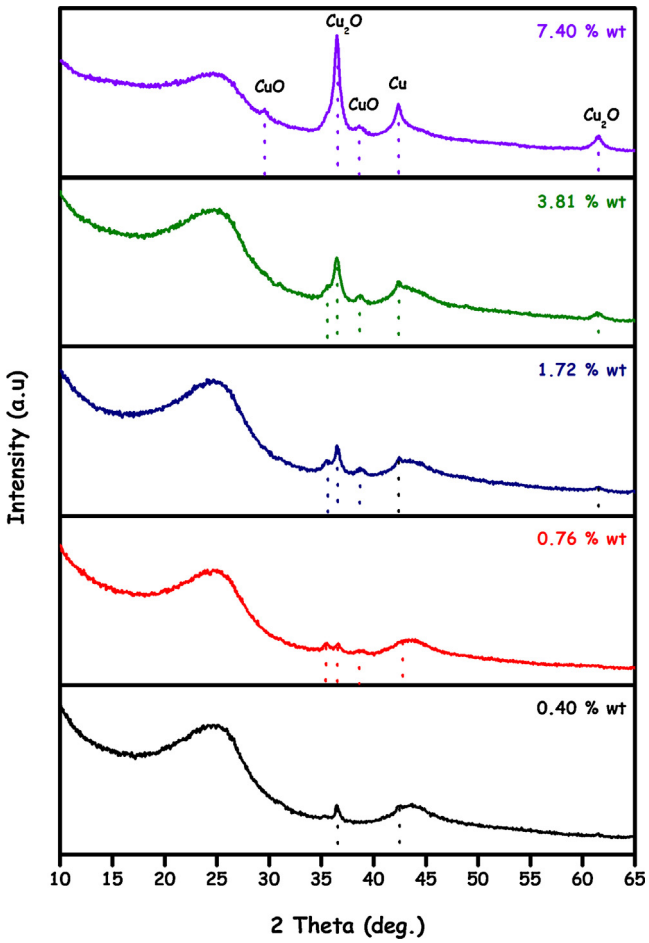

Fig. 1. The powder X-ray diffraction (P-XRD) patterns of Cu–Cu_2O–CuO/C samples with various copper loadings (wt% = 0.40, 0.76, 1.72, 3.81, 7.4 as determined by ICP-OES).

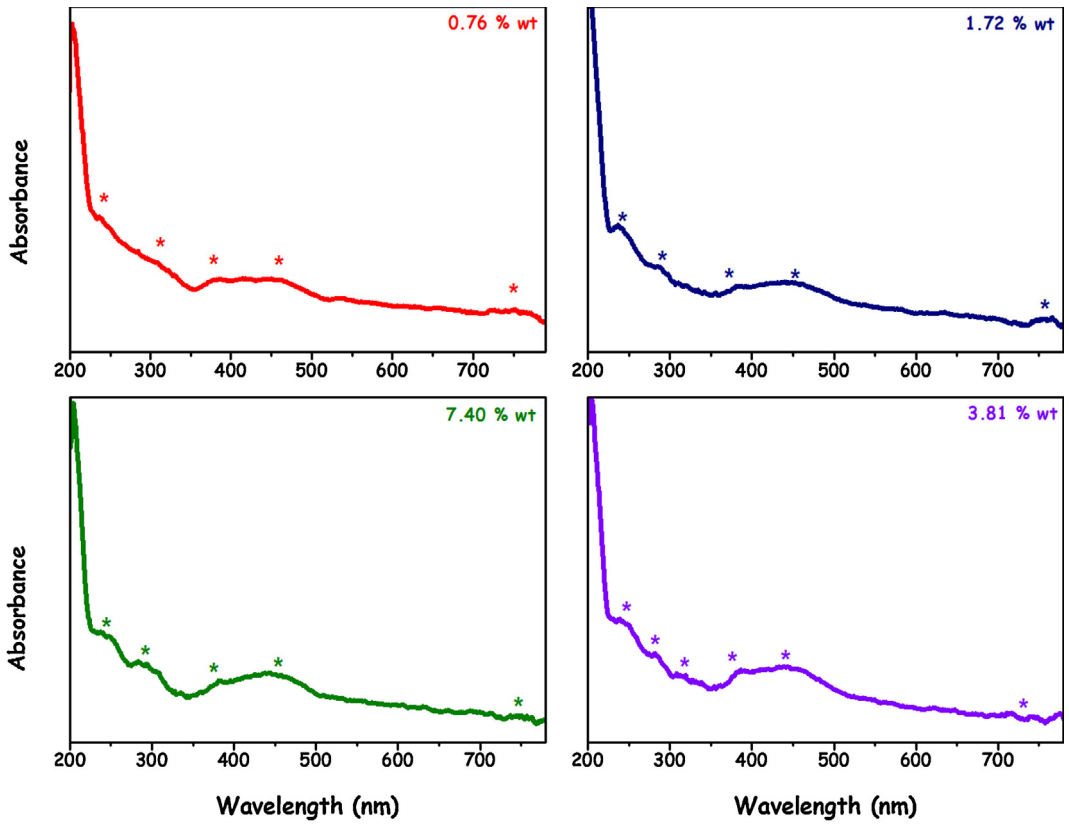

Fig. 2. The diffuse reflectance UV–vis absorption (DR-UV/vis) spectra in the range of 200–780 nm for Cu–Cu_2O–CuO/C samples with various copper loadings (wt% = 0.76, 1.72, 3.81, 7.4; the asterisks (*) shows the positions of the bands).

2.3. Preparation of Cu–Cu_2O–CuO/C Catalyst

In a typical experiment, 5.0 mL of 44.5 μmol aqueous copper solution (7.6 mg $CuCl_2.2H_2O$) is mixed with activated carbon (280 mg) at 400 rpm for 2 h. Then, 1.0 mL aqueous solution of $NaBH_4$ (25.6 mg, 0.55 mmol) was added to this mixture and the resulting solution was stirred for half an hour under air at room temperature. After centrifugation (6000 rpm, 5 min.), copious washing with water (3× 20 mL), filtration, and drying in vacuum oven at 150 °C under 10^{-2} Torr, Cu–Cu_2O–CuO/C catalyst was obtained as powder and stored under argon atmosphere.

2.4. Determination of the Catalytic Activity of Cu/Cu_2O/CuO@C Catalyst in the Methanolysis of Ammonia–borane

The catalytic activity of Cu–Cu_2O–CuO/C in the methanolysis of AB was determined by measuring the rate of hydrogen generation. The volume of released gas during the reaction was monitored using the gas buret by water displacement. Before starting the catalytic activity test, a jacketed one necked reaction flask (50.0 mL) containing a Teflon-coated stir bar was placed on a magnetic stirrer (Heidolph MR-3004) and thermostated to 25 °C by using a constant temperature bath (Lab Companion RW-0525). In a typical experiment, Cu–Cu_2O–CuO/C catalyst was weighed and transferred into the reaction flask, and then 4.0 mL CH_3OH was added into the reaction flask under argon purging and this mixture was stirred for 15 min. to achieve thermal equilibrium. Next, 1.0 mL CH_3OH solution of AB (17.5 mg, 0.5 mmol) was added into the reaction flask via its septum by using a 1.0 mL gastight syringe and the catalytic reaction was started (t = 0 min) by stirring the mixture at 600 rpm.

3. Results and discussion

3.1. Preparation and Characterization of Cu–Cu_2O–CuO/C Catalyst

Cu–Cu_2O–CuO/C catalyst was simply and reproducibly prepared by wet-impregnation followed by simultaneous reduction method [31]. Typically, an aqueous solution containing copper(II) chloride and activated carbon was mixed to impregnate $CuCl_2$ on carbon surface. Next, sodium borohydride as a reducing agent was added to this mixture and the resulting solution was stirred for half an hour under air at room temperature. After centrifugation, copious washing with water, and dehydrated in vacuum oven at 150 °C under 10^{-2} Torr, Cu–Cu_2O–CuO/C catalyst was obtained as dark gray powder and characterized by ICP-OES, XRD, XPS, Raman, DR-UV/vis, BFTEM, and HRTEM.

Fig. 1 depicts P-XRD patterns of dehydrated Cu–Cu_2O–CuO/C samples with various copper loadings (wt% = 0.40, 0.76, 1.72, 3.81, 7.4 as determined by ICP-OES), which reveal that the crystalline nature of Cu, Cu_2O and CuO NPs. The diffraction peaks at 29.5° (CuO [1 1 0]), 35.6° (CuO [1 1 1]), 36.5° (Cu_2O [1 1 1]), 38.7° (CuO [2 0 0]), 42.2° (Cu [1 1 1]) and 61.5° (Cu_2O [2 2 0]) confirm that our catalytic material contains Cu, Cu_2O and CuO as all these assigned peaks match with the reported data for Cu (JCPDS No. 85-1326), Cu_2O (JCPDS No. 78-2076) and CuO (JCPDS No. 48-1548) [32]. The crystalline sizes of Cu, Cu_2O and CuO NPs were estimated to be 3.4, 4.6 and 2.9 nm from the Scherrer formula [33], which are in the range of particle sizes found by BFTEM analyses, vide infra.

The diffuse reflectance UV–vis absorption spectra of the samples at different copper loadings (wt% = 0.76, 1.72, 3.81, 7.4) are given in Fig. 2. The surface plasmon resonance band for Cu nanoparticles around 540 nm [34] was observed for only 0.76 wt%

Cu loaded sample, which almost disappeared in 1.72, 3.81, 7.4 wt% Cu loadings. On the other hand, the notable bands at 245, 290, 380, 454 nm and >600 nm are observed and they gain intensity as the copper loading of Cu–Cu_2O–CuO/C catalyst increases. The absorption bands around 245, 290, 380 and 454 nm can readily be attributed to band-to-band transitions in the Cu_2O nanoparticles [35–38] and the broad absorption feature at >600 nm is assignable to d–d transitions in Cu^{2+} in distorted octahedral surrounding by oxygen in CuO particles [35–38].

The evidence in both P-XRD and the optical profile of the presence of stable Cu_2O–CuO nanoparticles in our catalyst was also warranted (with a molar ratio of Cu_2O/CuO = 0.7) in-depth investigation by X-ray photoelectron spectroscopic measurements. XPS is a powerful technique for the study of transition metal compounds having localized valence d orbitals. In CuO, copper exists in (+2) oxidation state having mainly d^9 character. The XPS detected Cu $2p_{3/2}$ peak at 935 eV and the deconvulation of this peak (Fig. 3) disclosed a main peak at 934.9 eV and was accompanied by a series of satellites at 936.1, 941.5 and 944 eV. The main peak at 934.9 eV can be assigned to Cu^+ in Cu_2O and the shake-up satellite peak are evident and diagnostic of an open $3d^9$ shell, corresponding to Cu^{2+} in CuO [35,36,39]. The fact that Cu phase is observed in XRD (in all wt% Cu loadings) while the XPS and diffuse reflectance UV–vis absorption spectra indicate the absence of Cu(0) (>0.76 wt% Cu loading) implies the existence of copper oxide phases (CuO and Cu_2O) most probably as a thin film on the surface of copper(0) nanoparticles as all the latter techniques are surface sensitive. As the loading of copper (wt%) increases, the amount of stable oxide forms of copper increases and they cover the surface of copper(0) nanoparticles and hinder the observation of surface plasmon resonance band for Cu(0) nanoparticles [40,41].

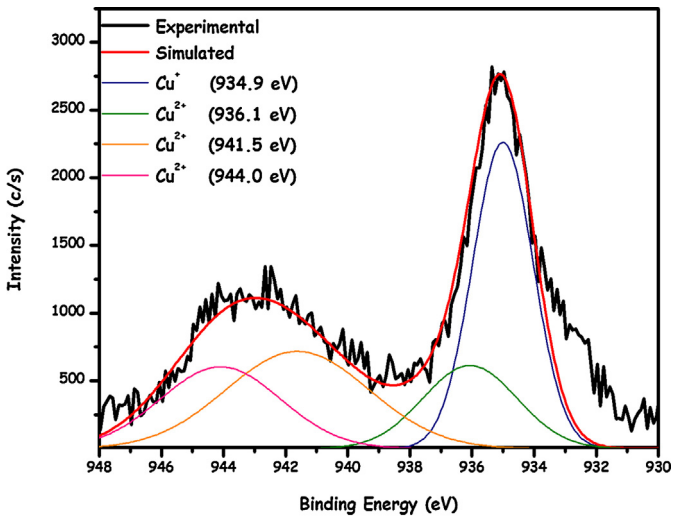

Fig. 3. The X-ray photoelectron spectrum of Cu–Cu_2O–CuO/C sample (0.76 wt% Cu) in the region of 930–948 eV and its simulated deconvulation.

The size and morphology of Cu–Cu_2O–CuO NPs were investigated by BFTEM and HRTEM, analyses. BFTEM images of Cu–Cu_2O–CuO/C catalyst (0.76 wt% Cu) in different magnifications are given in Fig. 4(a) and (b), which show the presence of well-dispersed Cu–Cu_2O–CuO NPs in the range of 1.5–8.7 nm with a mean diameter of 3.8 ± 1.7 nm (Fig. 4(c)). HRTEM image of Cu–Cu_2O–CuO/C given in Fig. 4(d) reveals that the highly crystalline nature of Cu–Cu_2O–CuO NPs and the lattice fringes were measured

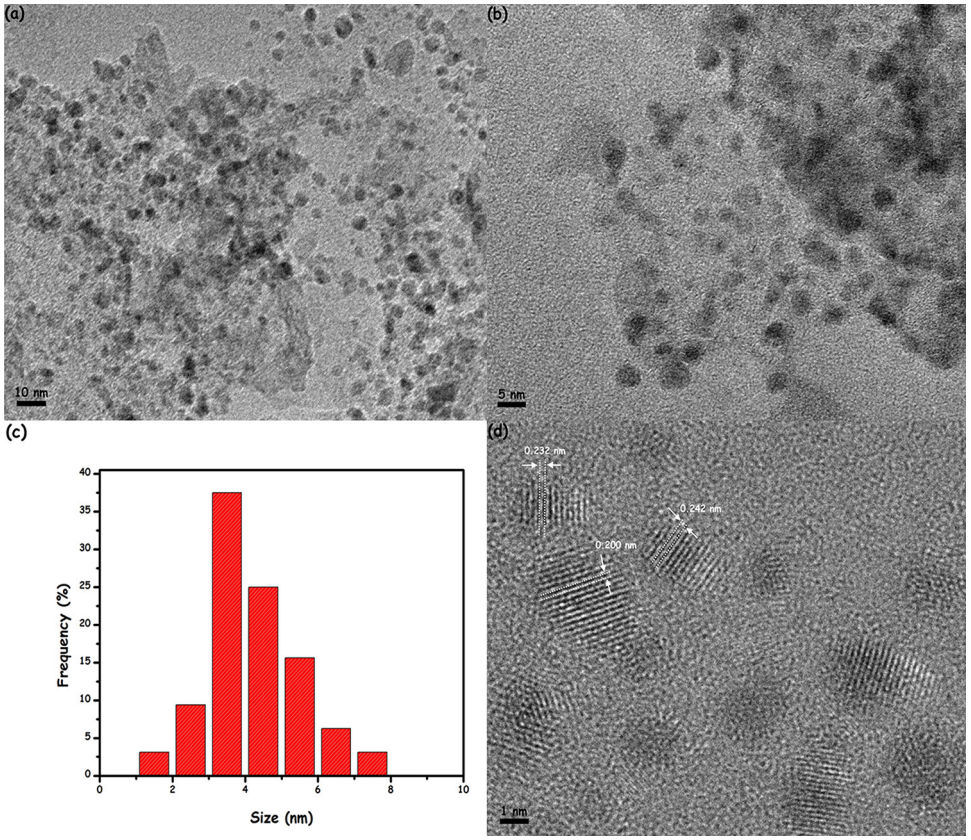

Fig. 4. (a and b) The conventional transmission microscopy (CTEM) images of Cu–Cu_2O–CuO/C catalyst (0.76 wt% Cu) in different magnifications, (c) the corresponding size histogram, (d) high resolution-TEM (HRTEM) image of Cu–Cu_2O–CuO/C catalyst (0.76 wt% Cu).

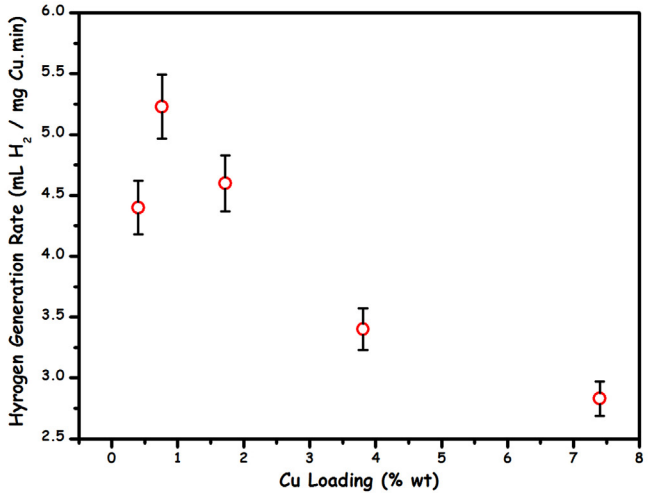

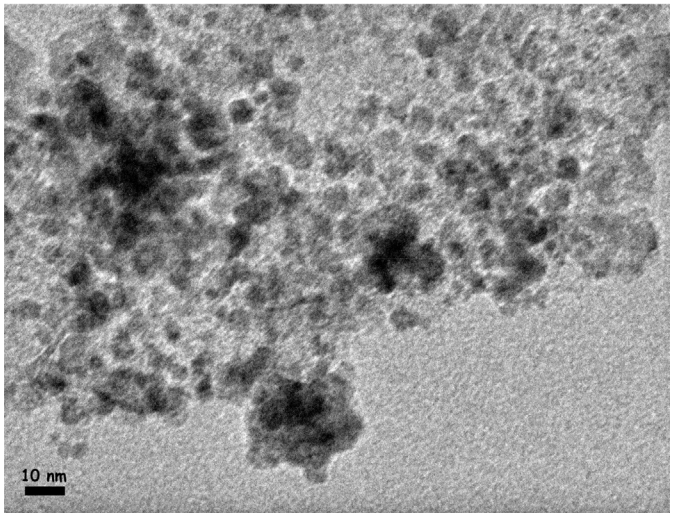

Fig. 5. The plot of hydrogen generation rate (mL H_2/(mg Cu min)) versus copper loadings (wt%) for Cu–Cu_2O–CuO/C catalyzed methanolysis of AB and CTEM image of Cu–Cu_2O–CuO/C catalyst with 7.4 wt% copper loading.

to be 0.200, 0.232 and 0.242 nm, which correspond to Cu (1 1 1) [42], CuO (2 0 0) [43] and Cu_2O (1 1 1) [44] spacings, respectively.

3.2. Cu–Cu_2O–CuO/C Catalyzed Methanolysis of Ammonia–borane

Firstly, in a series of experiment the catalytic activity of Cu–Cu_2O–CuO/C catalyst with various copper loadings in the range of 0.40–7.4 wt% Cu were tested in the methanolysis of AB at 25 °C to determine the effect of copper loading on Cu–Cu_2O–CuO/C activity. The hydrogen generation rates were found to be 4.4, 5.23, 4.60, 3.40 and 2.83 mL H_2 (mg Cu min)$^{-1}$ for Cu–Cu_2O–CuO/C catalysts containing 0.40, 0.76, 1.72, 3.81, 7.4 wt% Cu, respectively. The variation in catalytic activities reflects the change in the number of active sites of Cu–Cu_2O–CuO NPs. For example, BFTEM image of Cu–Cu_2O–CuO/C catalyst with 7.4 wt% Cu loading (Fig. 5(b)) shows the existence of agglomerates, which can explain the lowest activity observed at 7.4 wt% Cu loading. For all other test reactions performed in this study, samples of Cu–Cu_2O–CuO/C catalyst containing ~0.76 wt% Cu were used.

Fig. 6 shows the plots of H_2 (mol)/NH_3BH_3 (mol) versus time (min.) during the catalytic methanolysis of AB in the presence of Cu–Cu_2O–CuO/C catalyst in different copper concentrations at

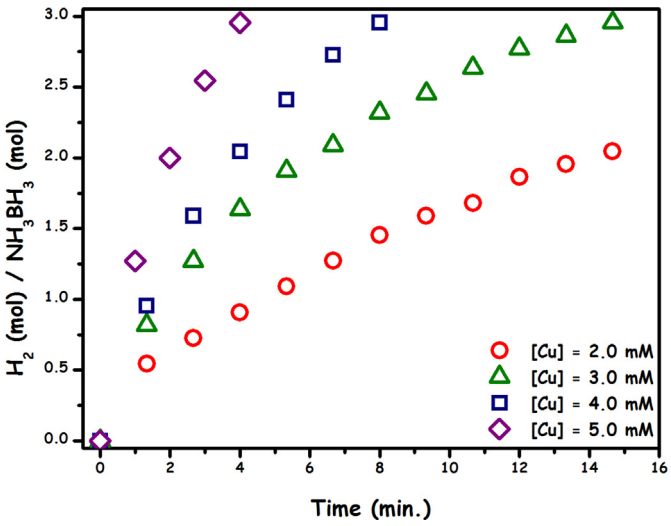

Fig. 6. The plot of H_2 (mol)/NH_3BH_3 (mol) versus time (min) graph for the methanolysis of AB ([AB] = 100 mM in 5.0 mL methanol) starting with different Cu–Cu_2O–CuO/C catalyst (0.76 wt% Cu) concentrations at 25 °C.

25 °C. As expected from preformed catalysts, a linear hydrogen generation starts without induction time period and continues until the complete consumption of AB. In addition to the volumetric measurement of the hydrogen gas evolution, the completion of methanolysis was also ascertained by using ^{11}B–{^1H} NMR spectroscopy. After the reaction, the signal of NH_3BH_3 at δ = 24.2 ppm (q) completely disappears and a new resonance at δ = 8.1 ppm (s) shows up, which is readily assigned to the [$B(OCH_3)_4$] anion.

It should be noted that, the complete conversion of AB is achieved by using % 3.0 mol Cu within 15 min at 25 °C. The reaction rates for each catalyst concentration were calculated from the linear portion of each plot. The logarithmic plot of the hydrogen generation rate versus catalyst concentration gives the line with a slope of 0.87 (Fig. S-1) indicative of the catalytic reaction is close to first-order with respect to the copper concentration. The *initial* turnover frequency (TOF) value for Cu–Cu_2O–CuO/C catalyst in the methanolysis of AB was found to be 24 min^{-1} at 25 °C. To the best of our knowledge this is the highest TOF value among the first row metal catalysts such as $CoCl_2$ (14 min^{-1}) [23], Cu@Cu_2O

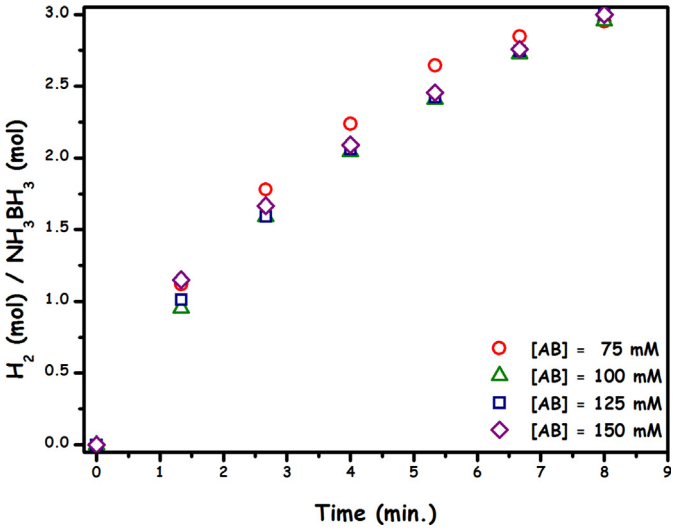

Fig. 7. The plot of H_2 (mol)/NH_3BH_3 (mol) versus time (min.) graph for Cu–Cu_2O–CuO/C (0.76 wt% Cu) catalyzed methanolysis of AB ([Cu] = 4.0 mM in 5.0 mL methanol) starting with different AB concentrations at 25 °C.

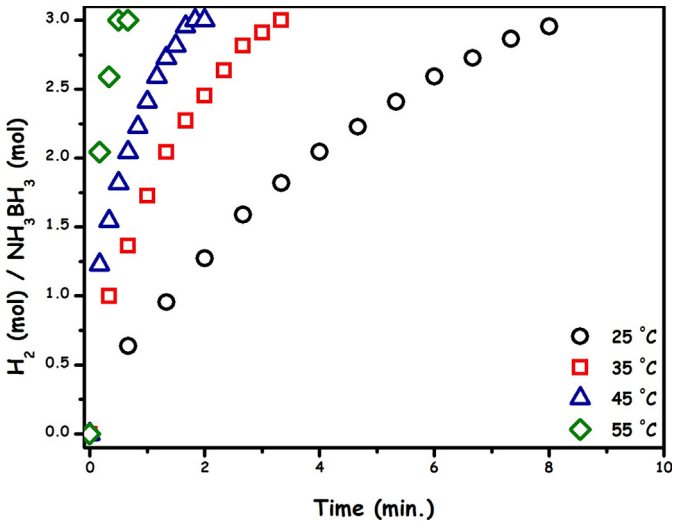

Fig. 8. The plot of H_2 (mol)/NH_3BH_3 (mol) versus time (min) graph for Cu–Cu_2O–CuO/C (0.76 wt% Cu) catalyzed methanolysis of AB ([AB] = 100 mM, [Cu] = 4.0 mM in 5.0 mL methanol) at different temperatures.

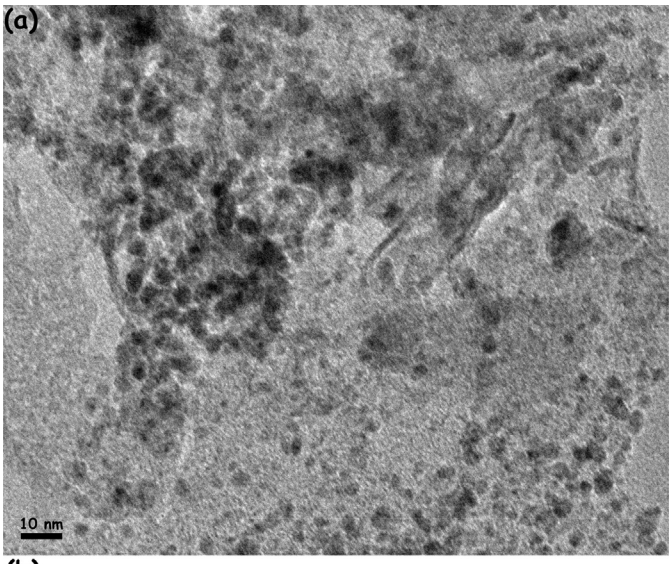

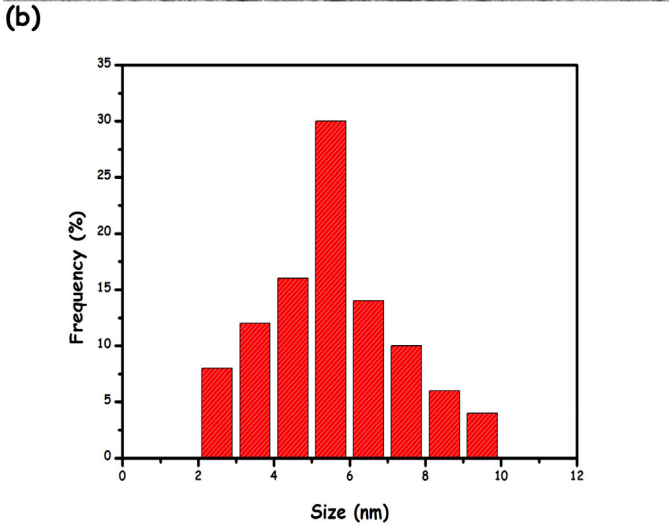

Fig. 10. (a) CTEM image and (b) corresponding size histogram of Cu–Cu_2O–CuO/C catalyst (0.76 wt% Cu) harvested after the eight catalytic recycle from the methanolysis of AB at 25 °C.

($0.1\ min^{-1}$) [24], Cu_2O ($0.2\ min^{-1}$) [24], Co–Co_2B ($7.5\ min^{-1}$) [25], Ni–Ni_2B ($5.5\ min^{-1}$) [25], Co–Ni–B ($10.5\ min^{-1}$) [25] tested in the methanolysis of AB at room temperature. Moreover, this *initial* TOF value is also comparable with that of obtained by some of the previously tested precious metal based catalysts; Pd-PVP ($23\ min^{-1}$) [26], CoPd/C ($28\ min^{-1}$) [28] and Rh-zeolite ($30\ min^{-1}$) [29]. In a set of control experiments the catalytic activities of bulk Cu, Cu_2O and CuO at the same copper concentration ([Cu] = 5.0 mM) have been tested in the methanolysis of AB at 25 °C (Fig. S-2). It was found that none of bulk Cu, Cu_2O and CuO provides reasonable activity and supported nano-sized Cu–Cu_2O–CuO mixture is the true kinetically competent catalyst in the methanolysis of AB.

The effect of substrate concentration on the hydrogen generation rate was also studied by performing a series of experiments starting with varying initial concentration of AB while the catalyst concentration is kept constant ([Cu] = 4.0 mM). Fig. 7 shows the plots of the volume of H_2 generated versus time during Cu/Cu_2O/CuO@C catalyzed methanolysis of AB for various initial concentrations of AB at 25 °C. As given in Fig. S-3 Cu–Cu_2O–CuO/C

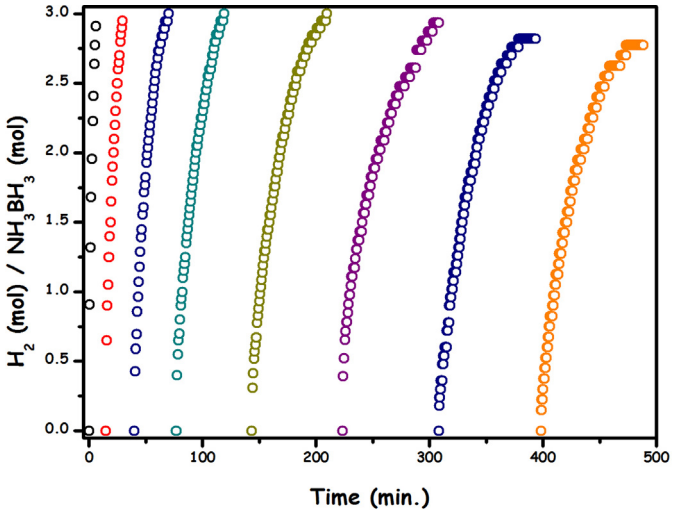

Fig. 9. The plot of H_2 (mol)/NH_3BH_3 (mol) versus time (min.) graph up to eight recycles for Cu–Cu_2O–CuO/C (0.76 wt% Cu) catalyzed methanolysis of AB ([AB] = 100 mM, [Cu] = 4.0 mM in 5.0 mL methanol) at 25 °C.

catalyzed methanolysis of AB was found to be zero-order with respect to substrate concentration at room temperature.

In addition to the effect of [Cu] and [NH_3BH_3] concentrations on the dehydrogenation rate, we also investigated the dehydrogenation rate depending on the temperature to find the activation parameters (E_a, $\Delta H^{\neq}$, $\Delta S^{\neq}$). For this purpose, Cu–Cu_2O–CuO/C catalyzed methanolysis of AB was carried out at different temperatures in the range of 25–55 °C. The plots of H_2 (mol)/NH_3BH_3 (mol) versus time (min.) for Cu–Cu_2O–CuO/C catalyzed methanolysis of AB at these temperatures are given in Fig. 8, it shows the increase in hydrogen generation rate in parallel to temperature increase. The values of observed rate constants k_{obs} determined from the nearly linear portions of the each plots at four different temperatures (Fig. 8) are used to plot Arrhenius and Eyring plots (Figs. S-4 and S-5) to calculate activation parameters: activation energy E_a = 67.9 kJ/mol, activation enthalpy $\Delta H^{\neq}$ = 65.4 kJ/mol and activation entropy $\Delta S^{\neq}$ = −24.8 J/mol K. This activation energy value is higher than that of previously found by Pd-PVP (35 kJ/mol) [26], CoPd/C (26 kJ/mol) [28], Rh-zeolite (40 kJ/mol) [29] and Ru-MMT (24 kJ/mol) [30] catalysts. The small value of activation enthalpy and the negative value of the activation entropy are implies

that an associative mechanism occurs in the transition state for Cu–Cu_2O–CuO/C catalyzed methanolysis of AB.

Aside from activity, the recyclability of Cu–Cu_2O–CuO/C catalyst was also examined in the methanolysis of AB. The recycling of Cu–Cu_2O–CuO/C catalyst was considered by performing Cu–Cu_2O–CuO/C catalyzed methanolysis of AB, in which when all of AB was converted to $NH_4B(OCH_3)_4$ and H_2, more AB was added into the solution and the reaction was continued in this way up to eight cycles (Fig. 9). It was found that Cu–Cu_2O–CuO/C catalyst shows high stability in the course of the catalytic recycles and retains 76% of its initial activity and provides 94% of conversion at 8th recycle.

BFTEM analysis of Cu–Cu_2O–CuO/C catalyst harvested after 8th catalytic recycle (Fig. 10) show the increase in the size of Cu–Cu_2O–CuO NPs (5.7 ± 2.3 nm), which explains the decrease observed in the activity of Cu–Cu_2O–CuO/C catalyst at 8th catalytic run. Moreover, ICP-OES analyses of isolated Cu–Cu_2O–CuO/C catalyst and reaction solution from 8th catalytic recycle gave us (i) almost the identical copper amount with that of the fresh catalyst and (ii) no leaching of metals into the reaction solution. Additionally, the methanolysis of AB can completely be stopped by removing Cu–Cu_2O–CuO/C catalyst from the reaction solution. The sum of these results is indicative of the high stability of Cu–Cu_2O–CuO NPs against to sintering and leaching throughout the catalytic runs in the AB methanolysis.

4. Conclusions

In summary, our study of the preparation and characterization of Cu–Cu_2O–CuO/C catalyst for the methanolysis of ammonia–borane has led to the following conclusions and insights. Cu–Cu_2O–CuO/C catalyst can easily and reproducibly prepared by a simple deposition-reduction technique without using any stabilizer in water at room temperature. Cu–Cu_2O–CuO/C (0.76 wt% Cu) was found to be highly active nanocatalyst in the methanolysis of ammonia–borane. They provide exceptional *initial* turnover frequency (TOF = 24 min^{-1}), which is the highest TOF value among the first row metal catalysts employed in the same reaction at room temperature. Moreover, the complete release of hydrogen is achieved even in successive recycles. Cu–Cu_2O–CuO NPs show exceptional stability throughout the catalytic runs against leaching and sintering so that they retain 76% of their initial activity even at 8th catalytic recycle. Overall, Cu–Cu_2O–CuO/C catalyst is available by a simple and low cost procedure and is found to be exceptional catalyst in terms of activity and stability in the methanolysis of ammonia–borane. Therefore, it is worth to testing them as catalysts in applications of hydrogen supply by using ammonia–borane as solid hydrogen storage material.

Acknowledgments

The partial supports by Fevzi Akkaya Scientific Activities Support Fund (FABED), Science Academy and Turkish Academy of Sciences (TUBA) are gratefully acknowledged.

Appendix A. Supplementary data

Supplementary data associated with this article can be found, in the online version, at http://dx.doi.org/10.1016/j.apcatb.2014.10.011.

References

[1] J. Graetz, Chem. Soc. Rev. 38 (2009) 73–82.
[2] N.Z. Muradova, T.N. Veziroglu, Int. J. Hydrogen Energy 30 (2005) 225–237.
[3] J.A. Turner, Science 285 (1999) 687–689.
[4] L. Schlaphach, A. Zuttel, Nature 414 (2001) 353–358.
[5] J. Turner, G. Sverdrup, K. Mann, P.G. Maness, B. Kroposki, M. Ghirardi, R.J. Evans, D. Blake, Int. J. Energy Res. 32 (2008) 379–386.
[6] S.H. Lim, J. Luo, Z. Zhong, W. Ji, J. Lin, Inorg. Chem. 44 (2005) 4124–4126.
[7] J. Weitkamp, M. Fritz, S. Ernst, Int. J. Hydrogen Energy 20 (1995) 967–973.
[8] N.B. McKeown, P.M. Budd, Chem. Soc. Rev. 35 (2006) 675–690.
[9] N.L. Rossi, J. Eckert, M. Eddaoudi, D.T. Vodak, J. Kim, M. O'Keefe, O.M. Yaghi, Science 300 (2003) 1127–1134.
[10] M. Au, A. Jurgensen, J. Phys. Chem. B 110 (2006) 7062–7067.
[11] M. Zahmakiran, S. Özkar, Langmuir 25 (2009) 2667–2676.
[12] E. Rönnebro, E.H. Majzoub, J. Phys. Chem. B 111 (2007) 12045–12052.
[13] H.L. Jiang, S.K. Singh, J.M. Yan, X.B. Zhang, Q. Xu, ChemSusChem 3 (2010) 541–548.
[14] H.L. Jiang, Q. Xu, Catal. Today 170 (2011) 56–63.
[15] T. Umegaki, J.M. Yan, X.B. Zhang, H. Shioyama, N. Kuriyama, Q. Xu, Int. J. Hydrogen Energy 34 (2009) 2303–2311.
[16] M. Yadav, Q. Xu, Energy Environ. Sci. 5 (2012) 9698–9725.
[17] S. Karahan, M. Zahmakiran, S. Özkar, Int. J. Hydrogen Energy 36 (2011) 4958–4964.
[18] C.W. Hamilton, R.T. Baker, A. Staubitz, I. Manners, Chem. Soc. Rev. 38 (2009) 279–295.
[19] G. Wolf, J. Baumann, F. Baitalow, F.P. Hoffmann, Thermochim. Acta 343 (2000) 19.
[20] C.A. Jaska, K. Temple, A.J. Lough, I. Manners, J. Am. Chem. Soc. 125 (2003) 9424.
[21] M. Zahmakiran, S. Özkar, Top. Catal. 56 (2013) 1171–1183.
[22] K.V. Kordesch, G.R. Simader, Chem. Rev. 95 (1995) 191–207.
[23] V.P. Ramachandran, D.P. Gagare, Inorg. Chem. 46 (2007) 7810–7817.
[24] S.B. Kalidindi, U. Sanyal, B.R. Jagirdar, Phys. Chem. Chem. Phys. 10 (2008) 5870–5874.
[25] S.D. Kalidindi, A.S. Vernekar, B.R. Jadirgar, Phys. Chem. Chem. Phys. 11 (2009) 770–775.
[26] H. Erdoğan, Ö. Metin, S. Özkar, Phys. Chem. Chem. Phys. 11 (2009) 10519–10525.
[27] H. Erdoğan, Ö. Metin, S. Özkar, Catal. Today 170 (2011) 93–98.
[28] D. Sun, V. Mazumder, Ö. Metin, S. Sun, ACS Catal. 2 (2012) 1290–1295.
[29] S. Çaliskan, M. Zahmakiran, S. Özkar, Appl. Catal. B: Environ. 93 (2010) 387–394.
[30] H.B. Dai, X.D. Kang, P. Wang, Int. J. Hydrogen Energy 35 (2010) 10317–10323.
[31] R.J. White, R. Luque, V.L. Budarin, J.H. Clarka, D.J. Macquarrie, Chem. Soc. Rev. 38 (2009) 481.
[32] Joint Committee on Powder Diffraction Standards, JCPDS International Center for Diffraction Data, Pennsylvania, 1991.
[33] H.P. Klugg, L.E. Alexander, X-Ray Diffraction Procedures, Wiley, New York, 1954.
[34] A.N. Pestryakov, V.P. Petranovskii, A. Kryazhov, O. Ozhereliev, N. Pfänder, A. Knop-Gerick, Chem. Phys. Lett. 385 (2004) 173–176.
[35] M. Zahmakiran, S. Özkar, Mater. Lett. 63 (2009) 1033–1036.
[36] M. Zahmakiran, S. Özkar, T. Kodaira, T. Shiomi, Mater. Lett. 63 (2009) 400–402.
[37] K. Borgohain, N. Murase, S. Mahanumi, J. Appl. Phys. 92 (2002) 1292–1298.
[38] A. Pestryakov, V.P. Petranovski, A. Kryazhov, O. Ozhereliev, N. Pfander, A. Knop-Gericke, Chem. Phys. Lett. 385 (2004) 173–179.
[39] S.K. Chawia, N. Sankarraman, J.H. Payer, J. Electron Spectrosc. Relat. Phenom. 61 (1992) 1–8.
[40] M. Zahmakiran, S. Ozkar, Mater. Lett. 63 (2009) 1033–1036.
[41] V.R. Palkar, P. Ayyub, S. Chattopadhyay, M. Multani, Phys. Rev. B 53 (1996) 2167–2174.
[42] G. Cheng, A.G.H. Walker, Anal. Bioanal. Chem. 396 (2010) 1057–1069.
[43] H.Q. Wu, X.W. Wei, M.W. Shao, J.S. Gu, M.Z. Qu, Chem. Phys. Lett. 364 (2002) 152–156.
[44] W.Z. Wang, G.H. Wang, X.S. Wang, Y.J. Zhan, Y.K. Liu, C.L. Zheng, Adv. Mater. 14 (2002) 67–69.